nature nanotechnology

ARTICLES

PUBLISHED ONLINE: 28 JUNE 2009 | DOI: 10.1038/NNANO.2009.153

Self-assembled cationic peptide nanoparticles as an efficient antimicrobial agent

Lihong Liu[1,4], Kaijin Xu[2], Huaying Wang[2], Jeremy Tan P. K.[1], Weimin Fan[2,3], Subbu S. Venkatraman[4], Lanjuan Li[2]* and Yi-Yan Yang[1]*

Antimicrobial cationic peptides are of interest because they can combat multi-drug-resistant microbes. Most peptides form α-helices or β-sheet-like structures that can insert into and subsequently disintegrate negatively charged bacterial cell surfaces. Here, we show that a novel class of core–shell nanoparticles formed by self-assembly of an amphiphilic peptide have strong antimicrobial properties against a range of bacteria, yeasts and fungi. The nanoparticles show a high therapeutic index against *Staphylococcus aureus* infection in mice and are more potent than their unassembled peptide counterparts. Using *Staphylococcus aureus*-infected meningitis rabbits, we show that the nanoparticles can cross the blood–brain barrier and suppress bacterial growth in infected brains. Taken together, these nanoparticles are promising antimicrobial agents that can be used to treat brain infections and other infectious diseases.

Brain inflammatory diseases such as meningitis and encephalitis are among the top ten infectious causes of death[1], and are caused by bacteria such as *Bacillus anthrax*, *Bacillus subtilis*[2,3] or *Staphylococcus aureus*, fungi or viruses. HIV-infected patients can easily contract fungi because of their damaged immune systems. *Candida albicans* is the most frequently found fungus in meningitis[4,5]. Satratoxin G from *Stachybotrys chartarum* has also been reported to cause brain inflammation[6]. Compared with fungal and bacterial infection, viral infection is the least severe in most cases. The patients usually recover with no long-term effects or sequelae after treatment with conventional antiviral drugs. Bacterial infection is far more serious and progresses quickly. It may result in hearing loss, learning disability or brain damage. Despite antibiotic treatment, there is high mortality and morbidity because of the difficulty in delivering drugs across the blood–brain barrier (BBB) to the brain.

Cationic antimicrobial peptides have received increasing attention due to their broad-spectrum activities and ability to combat multi-drug-resistant microbes[7]. The antimicrobial activities of most peptides depend upon the formation of α-helical[8–10] or β-sheet-like tubular[11] structures upon interaction with negatively charged cell surfaces or the formation of α-helical bundles after self-association in solution[12], followed by insertion into the cell membrane after recruiting additional peptide monomers, and disintegrating the cell membrane.

The TAT (YGRKKRRQRRR) peptide is the minimal amino-acid sequence required for membrane translocation, and was found in the transcriptional activator TAT protein of the human immunodeficiency virus type-1 (HIV-1)[13,14]. Chemical attachment of TAT onto proteins[15], siRNA[16] and liposomes[17] increased cellular uptake of proteins and genes. It has also been reported that after conjugation with TAT, proteins with molecular weights ranging from 36 to 119 kDa[18], quantum dots[19] and polymeric micelles[20] were able to cross the BBB. In this study, we design a short amphiphilic peptide (CG_3R_6TAT), which contains a hydrophilic block of cell-penetrating peptide TAT and six arginine residues (R_6 or Arg_6) for adding more cationic charges to improve membrane translocation[21,22], and a hydrophobic block of cholesterol (C), because it has a well-documented ability to drive self-assembly of cholesterol-containing materials[23] and to improve membrane permeability of cholesterol-incorporated compounds[24,25] (Fig. 1a). A spacer of three glycine moieties (G_3 or Gly_3) is built in between to separate the two blocks. This peptide can easily form core–shell structured nanoparticles (micelles) having a hydrophobic cholesterol core and a hydrophilic cationic peptide shell with TAT molecules arranged towards the surrounding environment (Fig. 1b). The formation of nanoparticles is expected to increase the local density of positive charge and peptide mass, thereby enhancing the antimicrobial properties of the cationic peptide. In addition, the presence of TAT molecules on the surfaces may render these nanoparticles capable of crossing the BBB for the treatment of brain infection.

Results and discussion

Synthesis and characterization of CG_3R_6TAT nanoparticles. G_3R_6TAT was synthesized by a solid-phase method. CG_3R_6TAT was obtained by grafting cholesteryl chloroformate onto the N-terminus of the G_3R_6TAT. This peptide had a critical micelle concentration (CMC) of 31.6 mg l^{-1} (that is, 10.1 μM) in deionized (DI) water (see Supplementary Fig. S1). At concentrations above the CMC, it can easily self-assemble to form core–shell nanoparticles. Briefly, 10 mg of CG_3R_6TAT was dissolved in 3 ml of dimethyl sulphoxide (DMSO), and dialysed against 500 ml of DI water at room temperature (22 °C) for 24–48 h using a dialysis membrane with a molecular-weight cut-off (MWCO) of 1,000 (Spectra/Por 7, Spectrum Laboratories). The external water phase was replaced every 6 h. The resulting nanoparticles were freeze dried, and characterized by hydrodynamic diameter (D_h), gyration of diameter (D_g), aggregation number and zeta potential using a Brookhaven BI-200SM goniometer system and a Zetasizer (Malvern Instrument). The values of D_h, D_g, aggregation number and zeta potential were 177 ± 6 nm, 152 ± 8 nm, 91 and 55 ± 4 mV, respectively. The aggregation number of 91 proves that the

[1]Institute of Bioengineering and Nanotechnology, 31 Biopolis Way, Singapore 138669, Singapore, [2]State Key Laboratory for Diagnosis and Treatment of Infectious Diseases, First Affiliated Hospital, College of Medicine, Zhejiang University, 79 Qingchun Road, Hangzhou 310003, China, [3]Pathology and Laboratory Medicine, Medical University of South Carolina, Charleston, South Carolina 29425, USA, [4]School of Materials Science and Engineering, Nanyang Technological University, Singapore 639798, Singapore. *e-mail: yyyang@ibn.a-star.edu.sg; ljli@zju.edu.cn

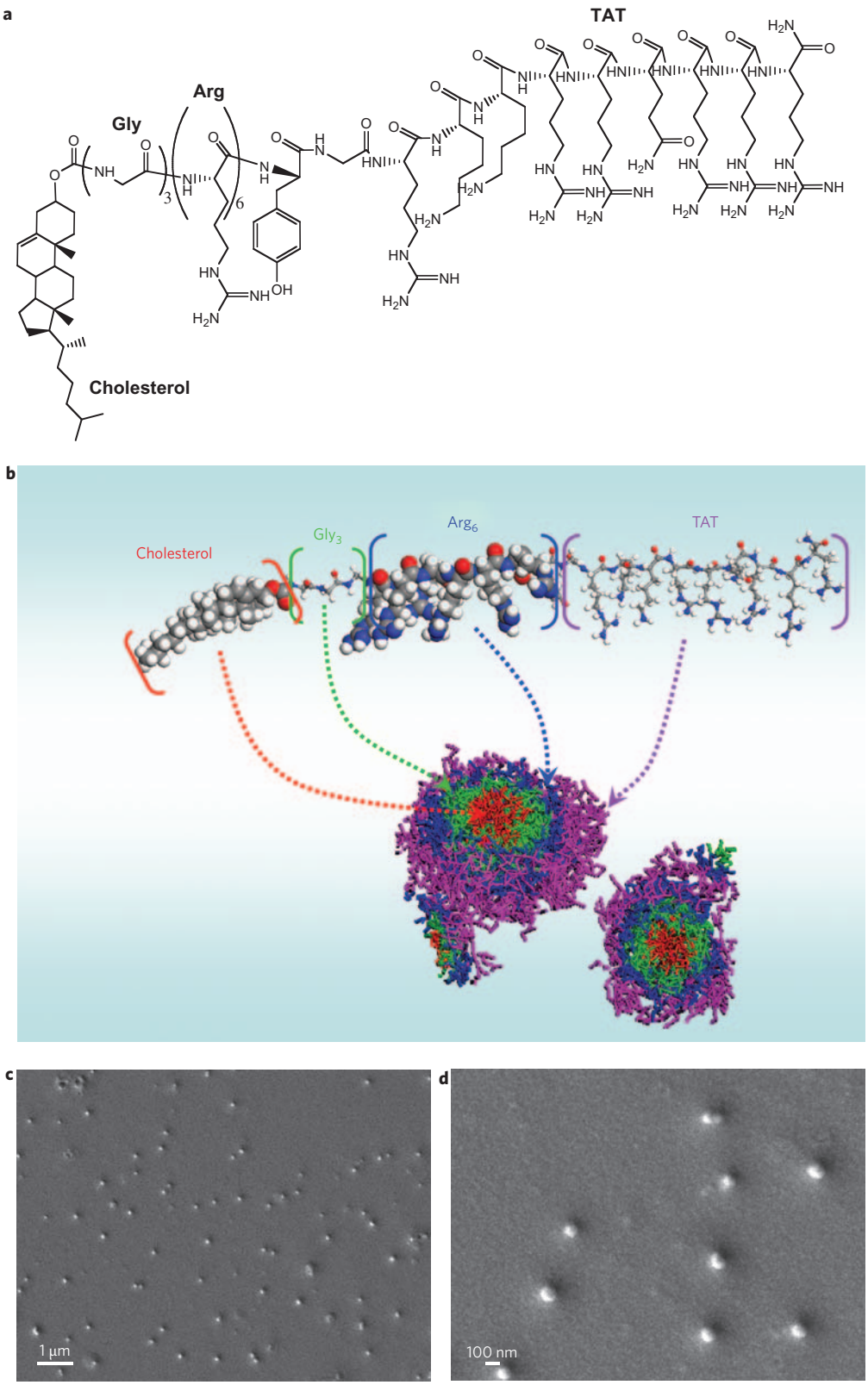

Figure 1 | Peptide structure and formation of peptide nanoparticles. a, Chemical structure of the designed peptide with cholesterol, glycine, arginine and TAT. **b**, Formation of micelles, simulated through molecular modelling using Materials Studio software. **c**,**d**, Scanning electron micrographs of nanoparticles.

formation of nanoparticles increases the local density of positive charge and peptide mass. A ratio of D_g/D_h close to 0.774 supports the formation of core–shell micelles, and any value equal to or bigger than 1 indicates the formation of vesicles or rod-like micelles[26,27]. The value of the oligopeptide nanoparticles (D_g/D_h) is 0.86, indicating the formation of core–shell micelles. The nanoparticles were spherical in nature and had a size less than 150 nm after self-drying under air (Fig. 1c,d). These positively

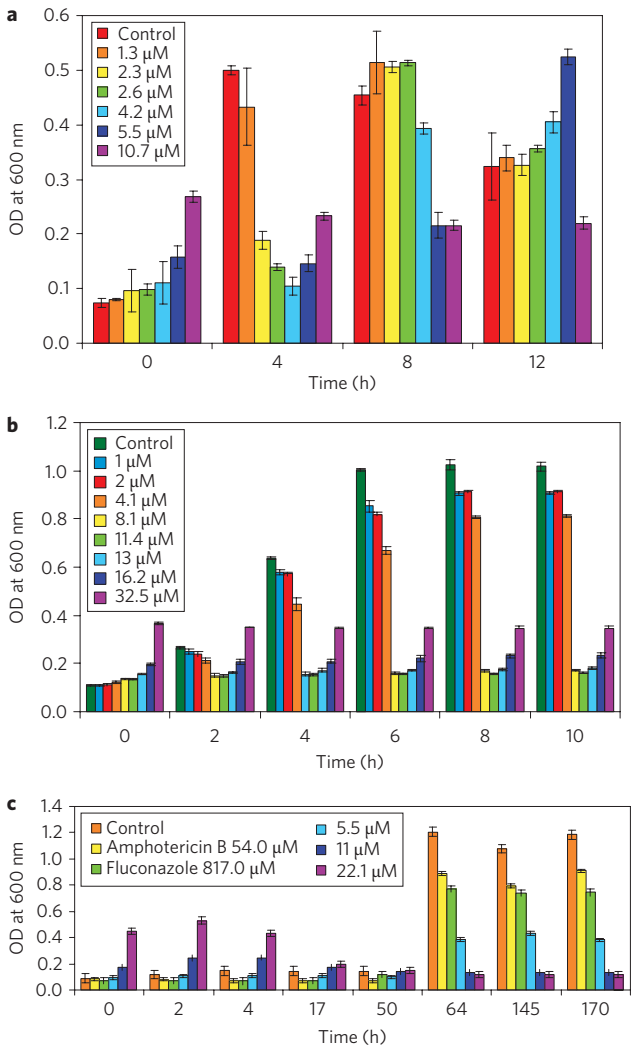

Figure 2 | Dose-dependent growth inhibition of *Bacillus subtilis*, *Cryptococcus neoformans* and *Stachybotrys chartarum*. **a**–**c**, Growth inhibition of *B. subtilis* (**a**), *S. aureus* (**b**) and *S. chartarum* (**c**) in the presence of CG_3R_6TAT peptide nanoparticles and conventional antifungal agents. The data are expressed as mean and standard deviations of at least three replicates. The standard deviation is shown by the error bars. OD, optical density.

charged nanoparticles may easily interact with the surfaces of microbes by means of electrostatic interaction.

***In vitro* antimicrobial properties of CG_3R_6TAT nanoparticles.** In clinical practice, patients with brain infections are empirically treated with antibiotics of broad-spectrum antimicrobial activity before identifying the specific pathogens, because any delay in treatment may cause mortality. Peptides, as potential antimicrobial agents for combating brain infections, must therefore be able to kill a variety of microbes including bacteria, drug-resistant bacteria, fungi and yeasts. We evaluated minimal inhibitory concentrations (MICs) of peptides and cationic peptide nanoparticles against *Staphylococcus aureus*, methicillin-resistant *Staphylococcus aureus* (MRSA), *Bacillus subtilis*, *Enterococcus faecalis*, vancomycin-resistant *Enterococcus*, *Streptococcus haemolyticus* (gram-positive bacteria), *Candida tropicalis* (yeast), *Candida albicans* 1 (clinical sample), *Candida albicans* (ATCC), *Cryptococcus neoformans* and *Stachybotrys chartarum* (fungus). The nanoparticles had a strong effectiveness against bacteria, and also against drug-resistant bacteria, yeast and fungi. Their MICs

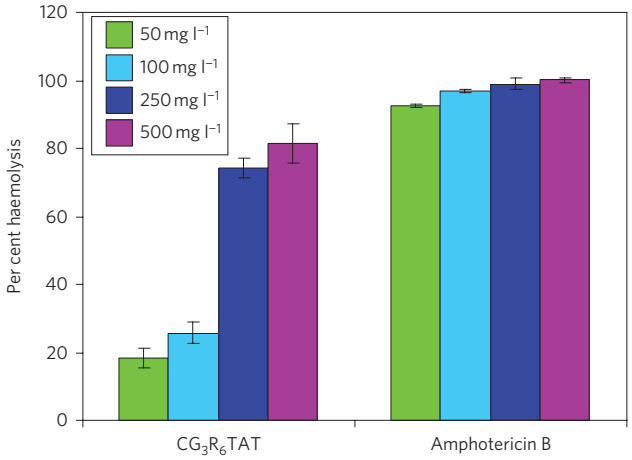

Figure 3 | Dose-dependent haemolytic activity of peptide nanoparticles compared with that of amphotericin B. The tests were repeated eight times, and the data are expressed as mean and standard deviations of eight replicates. The standard deviation is shown by the error bars.

were cell-type dependent—*S. aureus* (8.1 μM), methicillin-resistant *S. aureus* (11.4 μM), *B. subtilis* (10.7 μM), *E. faecalis* (11.4 μM), vancomycin-resistant *Enterococcus* (4.1 μM), *S. haemolyticus* (2.0 μM), *C. albicans* 1 (13.0 μM), *C. albicans* (10.8 μM), *C. tropicalis* (13.0 μM), *C. neoformans* (8.1 μM) and *S. chartarum* (11.0 μM) (Fig. 2; see also Supplementary Fig. S2)—close to or even below the CMC of the peptide.

Although TAT was reported to possess an inhibitory activity against *C. albicans*[28], its inhibitory efficiency was low (for example, MICs of G_3TAT are 290.0 and 289.0 μM against *B. subtilis* and *C. albicans*, respectively; see Supplementary Fig. S3). However, adding six cationic arginine residues to G_3TAT (that is, G_3R_6TAT) reduced the MIC values by a factor of 2.9 (290.0 and 289.0 versus 75.0 μM for *B. subtilis* and *C. albicans*, respectively; see Supplementary Figs S3 and S4). In TAT peptide, there are six arginine residues. The addition of TAT to G_3R_6 did not merely provide six more arginine residues, as the MICs of G_3R_{12} against *B. subtilis* and *C. albicans* were much higher than that of G_3R_6TAT (242.0 and 145.5 versus 75.0 μM; see Supplementary Figs S4 and S5). The cell-penetrating property of the TAT sequence may play a role in providing the stronger antimicrobial activities. Although the inhibitory efficiency induced by TAT alone was low, the introduction of TAT to G_3R_6 strongly enhanced its antimicrobial activity (MIC of 75.0 versus >444.4 μM, an increase by a factor of more than 4.9; see Supplementary Figs S4 and S6). Therefore, the arginine residues and TAT peptide block are both necessary for the observed antimicrobial activities.

The MIC of G_3R_6TAT was much higher than that of the nanoparticles self-assembled from the amphiphilic peptide CG_3R_6TAT (10.7/10.8 versus 75.0 μM, six times higher). Most cationic peptides do not have a specific target in microbes, and they interact with microbial membranes based on electrostatic interaction. We believe that the high local density of peptide mass and positive charges on our nanoparticles may lead to greater electrostatic interactions with the bacterial membranes, which in effect translates to greater antimicrobial activities and lower MIC values. In addition, the nanoparticles were much more powerful in inhibiting proliferation of *S. chartarum* than the conventional antifungal agents fluconazole and amphotericin B (MIC of 11.0 μM versus >817.0 and >54.0 μM, respectively; Fig. 2c). Moreover, the nanoparticles were superior to the conventional antibiotics penicillin G and doxycycline in killing *B. subtilis* (MIC of 11.0 versus 1,074 and 13.5 μM, respectively; see Supplementary Fig. S7).

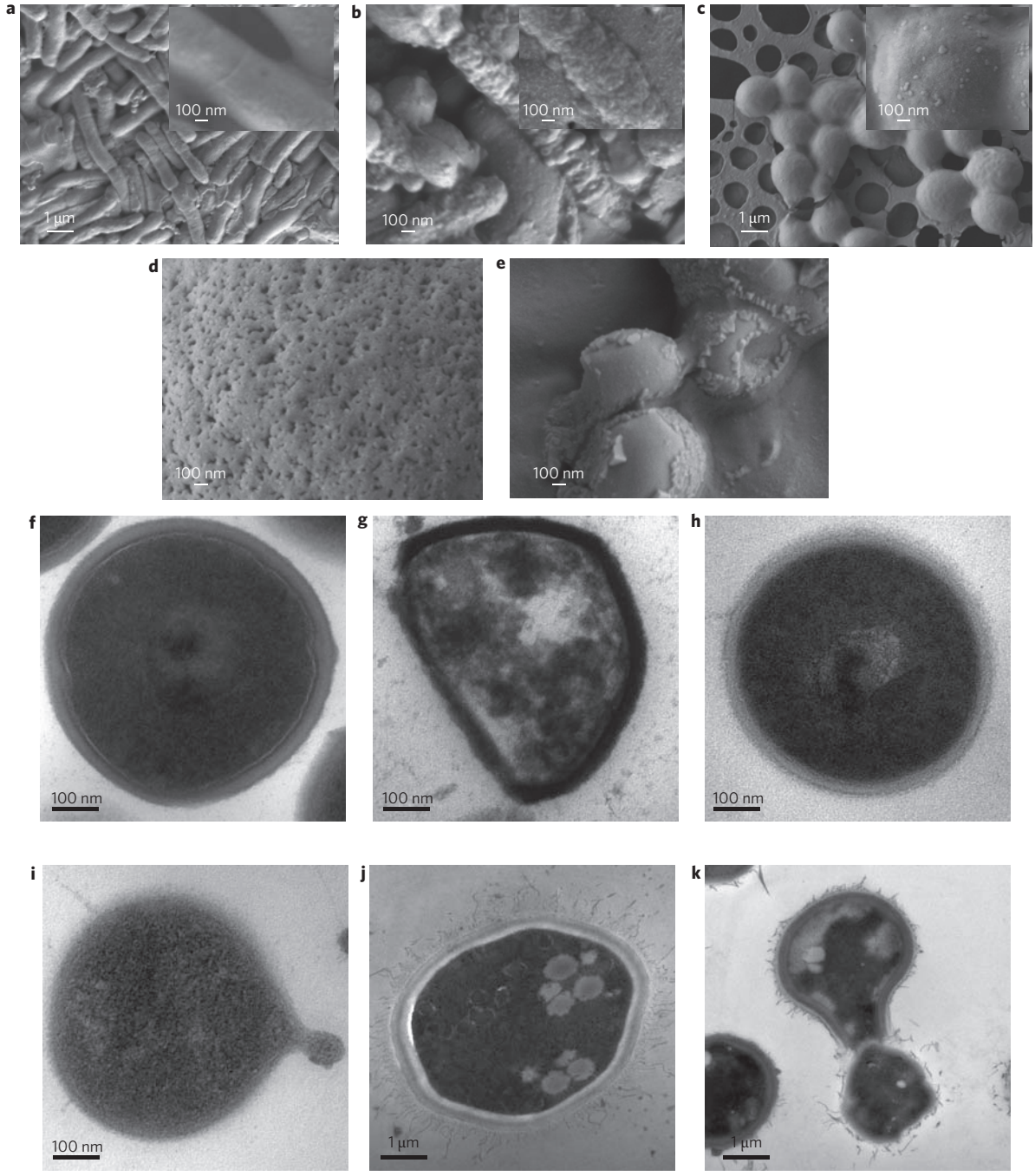

Figure 4 | Morphological studies of microorganisms before and after treatment with CG_3R_6TAT nanoparticles. a–e, SEM images of *B. subtilis* (**a**,**b**) and *C. albicans* (**c**–**e**) before (**a**,**c**) and after treatment with nanoparticles at 13.0 μM for 30 min (**d**), 90 min (**b**) and 100 min (**e**). Insets show enlarged views. **f–k**, TEM images of *S. aureus* (**f**,**g**), *E. faecalis* (**h**,**i**) and *C. neoformans* (**j**,**k**) before (**f**,**h**,**j**) and after (**g**,**i**,**k**) incubation with 32.0 μM of nanoaprticles for 2 h.

Haemolysis is one of the major side effects caused by many cationic peptides. The haemolysis of rat red blood cells was evaluated after incubation with the nanoparticles and amphotericin B. The nanoparticles demonstrated low haemolytic activity at low concentrations (Fig. 3). For example, at 16.0 μM (that is, 50 mg l^{-1}), a concentration higher than the MIC, less than 19% haemolysis was observed with the nanoparticles, whereas amphotericin B mediated more than 90% haemolysis at its MIC (54.0 μM, that is, 50 mg l^{-1}).

Proposed antimicrobial mechanism of CG_3R_6TAT nanoparticles. To understand the mechanism of the antimicrobial functions of the nanoparticles, we investigated morphological changes of various microorganisms before and after incubation with the nanoparticles at lethal doses for various periods of time through scanning electron microscopy (SEM) and transmission electron microscopy (TEM) observations. Untreated *B. subtilis* exhibited a smooth surface (Fig. 4a). In sharp contrast, the cell surface became rough after incubation with nanoparticles at a concentration of 13.0 μM for 90 min. In addition, a large number of minicells were formed, and cell debris was observed (Fig. 4b). The formation of minicells has been observed in *B. subtilis* treated with the cationic peptide antibiotic nisin[29]. The uptake of positively charged nanoparticles into the bacterial cell wall by means of non-specific electrostatic interaction accelerates cell

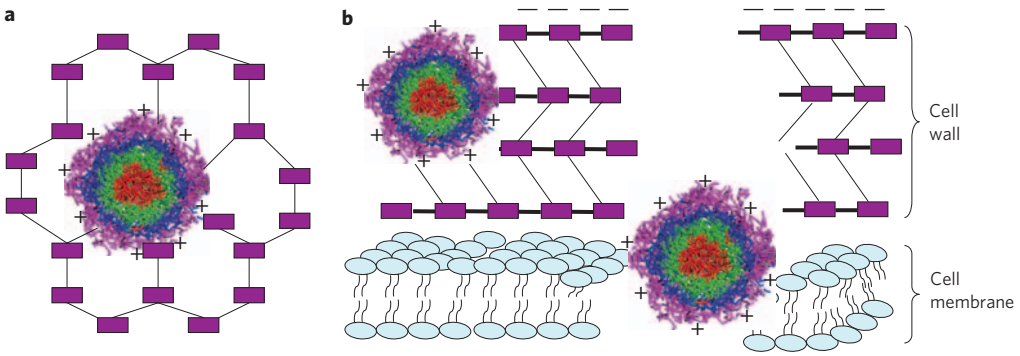

Figure 5 | A possible mechanism of antimicrobial nanoparticle activity. Uptake of nanoparticles through electrostatic interaction disintegrates the cell wall. They permeate the cell membrane due to their relatively large volume when compared to the thickness of the cell wall or cell membrane. **a**, Top view of a nanoparticle bound to the cell wall through electrostatic interaction. **b**, Cross-section of nanoparticles interacting with the cell wall and cell membrane. Nanoparticle: purple, TAT; blue, arginine; green, glycine; red, cholesterol.

division, which leads to the formation of minicells. It is possible that our nanoparticles may act in a similar way to nisin.

TEM images also show that the cell wall of *S. aureus* was broken and cell death was observed after incubation with 32 μM nanoparticles for 2 h (Fig. 4f,g). Under the same treatment, the cell walls of *E. faecalis* and *C. neoformans* were disrupted and lysis of the cells occurred (Fig. 4 h–k). The uptake of nanoparticles in the cell wall may cause the steric hindrance. In addition, there may be hydrogen binding/electrostatic interactions between the functional groups in the peptide and peptidoglycans of the cell wall, which are made from polymers of alternating *N*-acetylglucosamine and *N*-acetylmuramic acid in the β-linkage, crosslinked by short peptide stems. These two factors may work together to damage the cell wall and/or inhibit cell wall synthesis[30], resulting in osmotic lysis of the cells.

As shown in Fig. 4c–e, *C. albicans* also experienced morphological changes. Numerous pores of size less than 50 nm were formed on the cell surfaces after treatment with nanoparticles at a concentration of 13.0 μM for 30 min (Fig. 4c versus d). At 100 min, the cell wall was efficiently disrupted and protoplasts were exposed, which would eventually lead to cell lysis (Fig. 4e). In addition to the possible inhibition of cell wall synthesis or damage to the cell wall, the nanoparticles may permeate through the cytoplasmic membrane of the organisms due to the presence of TAT and/or the relatively large volume of the nanoparticles[4], thus destabilizing the membrane based on the electroporation and/or sinking raft model[31], resulting in cell death. Figure 5 shows a possible mechanism of antimicrobial nanoparticle activity.

***In vivo* anti-infective activity of CG_3R_6TAT nanoparticles.** To evaluate the *in vivo* anti-infective activity and toxicity level of the nanoparticles, *S. aureus* was introduced to mice intraperitoneally with a minimum lethal dose of 4.34×10^9 CFU ml^{-1} (CFU, colony forming unit; 0.5 ml), which was first determined from the survival rate of mice at 48 h after being challenged with different doses of the bacteria. At this lethal dose, 100% mice died within 48 h post-infection. Immediately after the challenge, the mice received intravenous injection of the peptide nanoparticles at various doses, and another injection at 24 h of the same doses. The mice were monitored for survival over a 7-day period after infection, and the ED_{50} (effective dose at which half the mice survive) of the peptide nanoparticles analysed by the method of BLISS was 0.35 mg kg^{-1}. In addition, the LD_{50} (lethal dose at which half the mice are killed) was determined to be 17.4 mg kg^{-1}. These results indicate that the peptide nanoparticles had a high therapeutic index (LD_{50}/ED_{50}, that is, 50) against *S. aureus* infection.

To determine whether the peptide nanoparticles can cross the BBB and kill bacteria in the brain, a *S. aureus*-induced meningitis rabbit model was used. The infected rabbits were treated with either vancomycin (conventional antibiotics) or peptide nanoparticles intravenously every 12 h, and the first dose was given at 12 h post-infection. Blood and cerebrospinal fluid (CSF) samples were taken from the auricular artery and intracisternal puncture, respectively, at different time points, and the percentage of neutrophils analysed. Brain tissues were removed at 48 h post-infection to determine the quantitative counts of *S. aureus* (CFUs). The decreased CFU, that is, reduced counts of *S. aureus* in the brain tissues at 36 h post-treatment with the nanoparticles proves that the peptide nanoparticles were able to penetrate the BBB and suppress bacterial growth in the brain (Fig. 6a). Neutrophils are the primary white blood cells that respond to a bacterial infection. The percentage of neutrophils is a parameter that is commonly used in the clinic to evaluate the degree of infection. A decreased percentage of neutrophils indicates a lower infection. As shown in Fig. 6b, the percentage of neutrophils in the peripheral blood was ~43–47% before infection, and increased to 85–89% at 12 h post-infection. Treatment with the nanoparticles or vancomycin reduced the percentage of neutrophils, which was 55–60% at 36 h post-treatment, whereas the percentage of neutrophils in the peripheral blood of the control group without any treatment was still 76% at this time point. Similarly, it was observed that treatment with nanoparticles or vancomycin also significantly decreased the percentage of neutrophils in the CSF (Fig. 6c). These findings indicate that treatment of the *S. aureus*-induced meningitis rabbits with nanoparticles suppressed bacterial growth and lowered the degree of the infection.

Meanwhile, alanine transaminase (ALT), aspartate transaminase (AST), total bilirubin, direct bilirubin, creatinine and urea nitrogen levels of the blood samples obtained from the meningitis rabbits with and without the treatment of the peptide nanoparticles at 48 h post-infection were measured to study the toxicity of the nanoparticles to the liver and kidneys. As listed in Supplementary Table S1, treatment with the nanoparticles did not elevate the levels of these key parameters, indicating that the nanoparticles did not cause significant damage to the liver and kidney functions at the tested dose.

The BBB is composed of a layer of endothelial cells held together by tight junctions (Fig. 6d), thus restricting the passage of substances (particularly water-soluble molecules or molecules larger than $M_r = 200–400$) from the bloodstream[32]. In general, there are two possible pathways for large water-soluble molecules to cross the BBB: specific receptor-mediated endocytosis (insulin, transferrin) and adsorptive endocytosis routes (cationic albumin and other plasma proteins)[32]. The cationic peptide nanoparticles synthesized in this study may be taken up by the BBB through adsorptive endocytosis, and then move into the CSF and diffuse into the brain tissues (Fig. 6d).

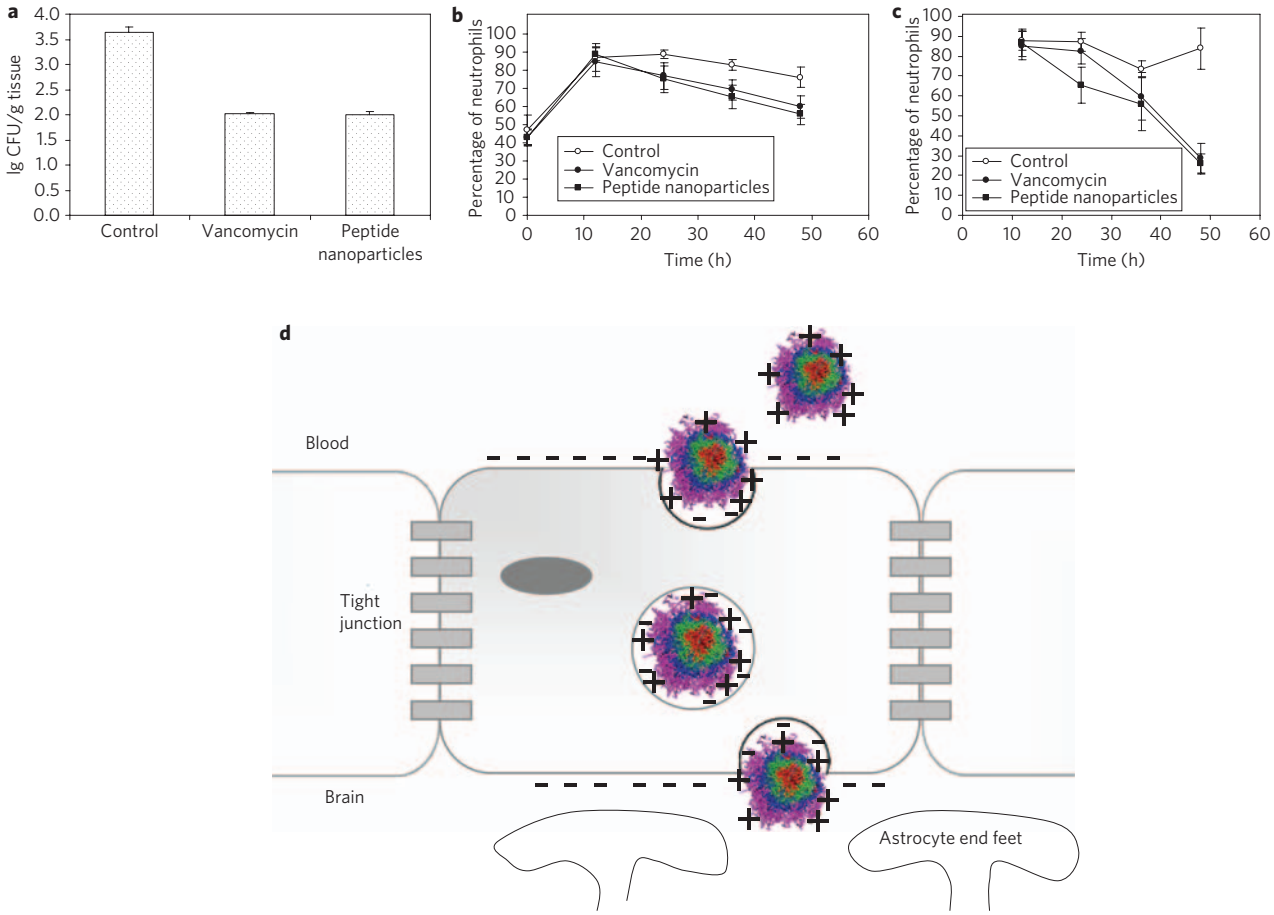

Figure 6 | Therapeutic effects of CG_3R_6TAT nanoparticles on *S.aureus*-induced meningitis rabbits. a, CFU of *S. aureus* in the brain tissues. **b**,**c**, Percentage of neutrophils in the blood (**b**) and the CSF (**c**). Data are expressed as mean and standard deviation as indicated by the error bars, based on values obtained from six rabbits. **d**, A possible mechanism through which peptide nanoparticles cross the BBB by means of adsorptive endocytosis. The nanoparticle is taken up by the BBB through adsorptive endocytosis, and then moves into the CSF and diffuses into the brain tissues. Nanoparticle: purple, TAT; blue, arginine; green, glycine; red, cholesterol.

Conclusions

In conclusion, we have designed and synthesized antimicrobial core–shell structured nanoparticles self-assembled from the amphiphilic peptide CG_3R_6TAT. We have demonstrated that the formation of nanoparticles strongly enhances its antimicrobial activities. These nanoparticles possess a broad spectrum of antimicrobial activities, which efficiently inhibit the growth of various types of gram-positive and drug-resistant gram-positive bacteria, fungi and yeast with low MIC values, yet induce relatively low haemolysis. In addition, they have a high therapeutic index (50) against *S. aureus* infection in a mouse model. Moreover, these peptide nanoparticles are able to cross the BBB in a *S. aureus*-induced meningitis rabbit model, and suppress bacterial growth in the brain. Importantly, they do not cause significant toxicity to the major organs, indicating that these nanoparticles may provide an efficient antimicrobial agent in treating brain infections. They may also be applied to other infectious diseases such as MRSA-associated infections and *C. albicans*-caused brain infections.

Methods

Peptide synthesis. G_3R_6TAT was synthesized according to the 9-fluorenylmethoxycarbonyl (Fmoc) approach using an Apex 396 peptide synthesizer (Aapptec). The peptide was assembled on Fmoc-Arg(Pbf)-Rink Amide-MBHA resin (LC Sciences) at the 0.1 mmol scale using a double coupling method. Briefly, resin was reacted with five equivalents of amino acids, five equivalents of activator reagent, benzotriazol-1-yl-oxytripyrrolidinophosphonium hexafluorophosphate (LC Sciences) and 10 equivalents of base, *N*-methylmorpholine (Merck). The Fmoc group was removed by gentle agitation in 20% of piperidine (Merck) in dimethylformamide (DMF, Sigma-Aldrich). After peptide synthesis, cleavage of the peptides from the resin was carried out with a mixture of trifluoroacetic acid (TFA, Merck), triisopropylsilane (Merck) and water in a volume ratio of 95:2.5:2.5 for 3–6 h. The solution was concentrated by rotary evaporation, followed by precipitation in cold diethyl ether (Sigma-Aldrich). The crude peptide was collected by filtration and dried under vacuum, and further purified using high-performance liquid chromatography (HPLC) consisting of a Waters 2767 sample manager, a Waters 996 PDA detector (Waters Corporation) and a GraceVydac C_{18} column (10 × 250 mm). The mobile phase was composed of water containing 0.1% TFA and acetonitrile containing 0.1% TFA, and the volume percentage of acetonitrile was gradually increased from 5 to 40% in 20 min at a flow rate of 8 ml min^{-1}. The peptide was characterized by analytical reverse-phase HPLC and matrix-assisted laser desorption ionization of time-of-flight (MALDI-TOF) mass spectrometry (Autoflex II, Bruker Daltronics) (see Supplementary Fig. S8). The purity of peptide was found to be about 95% according to HPLC analysis.

CG_3R_6TAT was obtained by grafting cholesteryl chloroformate onto G_3R_6TAT through the N-terminus. Briefly, cholesteryl chloroformate (Sigma-Aldrich, 148 mg) dissolved in 15 ml DMF was slowly added to 5 ml DMF containing 70 μl triethylamine (Fluka) and 88 mg of G_3R_6TAT at 0 °C with stirring. After 24 h of reaction, DMF was removed from the mixture by purging dry nitrogen gas, and the mixture was then precipitated with diethyl ether for three times to remove unreacted cholesteryl chloroformate. The crude product was further purified by dialysis against DMF for six days, followed by water for two days using a membrane with MWCO of 1,000 Da. Evidence of the successful synthesis of CG_3R_6TAT was obtained by MALDI-TOF and ^{1}H-NMR analyses (see Supplementary Figs S8 and S9).

Minimal inhibitory concentration (MIC) determination. *B. subtilius*, *S. aureus*, *C. albicans* and *S. chartarum* were obtained from ATCC. Methicillin-resistant *S. aureus*, *E. faecalis*, vancomycin-resistant *Enterococcus*, *S. haemolyticus*, *C. neoformans*, *C. tropicalis* and *C. albicans* 1 were extracted from patients' phlegm, and kindly provided by Y. S. Yu, Department of Infectious Diseases, The First Affiliated Hospital, College of Medicine, Zhejiang University, P.R. China. The bacteria were grown in tryptic soy broth or Mueller–Hinton broth for clinical

samples or Todd–Hewitt broth for *S. haemolyticus* at 37 °C. The yeast was cultured in yeast mould broth at 24 °C and the fungi were grown in tryptic soy broth at 26 °C. The MICs of the peptides, peptide nanoparticles or drugs were measured using a broth microdilution method. Briefly, 50 μl of peptide, peptide nanoparticle and drug solutions with various concentrations was placed into each well of 96-well plates. Microorganism solution (50 μl) at a concentration that gave an optical density reading of ~0.1–0.2 at 600 nm was added to each well. The optical density readings of microorganism solutions were measured as a function of time. The MIC was taken at the concentration at which no growth was observed with the unaided eye and microplate reader (Bio-Teck Instruments), and in the growing phase of the microorganisms. Broth containing cells alone was used as control. The tests were repeated at least three times.

***In vivo* studies.** All experiments involving animals were performed according to protocols approved by the Animal Studies Committee of P.R. China. Adult female ICR mice (~20 g) were used in all experiments for studies of LD_{50} and ED_{50}, and pathogen-free New Zealand rabbits (~2.5–3 kg) were used to establish the *S. aureus*-induced meningitis model. The detailed protocols for the *in vivo* studies are provided in the Supplementary Information.

Statistic analysis. Statistical analysis was performed using Student's *t*-test. Differences were considered statistically significant with probability $P < 0.05$.

Received 26 January 2009; accepted 14 May 2009; published online 28 June 2009

References

1. Obermaier, B., Klein, M., Koedel, U. & Pfister, H. W. Disease models of acute bacterial meningitis. *Drug Discov. Today* **3,** 105–112 (2006).
2. Ewald, C., Kuhn, S. & Kalff, R. Pyogenic infection of the central nervous system secondary to dental affection—a report of six cases. *Neurosurg. Rev.* **29,** 163–167 (2006).
3. Bert, F., Ouahes, O. & Lambert-Zechovsky, N. Brain abscess due to *Bacillus macerans* following a penetration periorbital injury. *J. Clin. Microbiol.* **33,** 1950–1953 (1995).
4. Jafari, H. S. *et al.* Effects of antifungal therapy on inflammation, sterilization and histology in experimental *Candida albicans* meningitis. *Antimicrob. Agents Chemother.* **38,** 83–89 (1994).
5. Casado, J. L. *et al.* Candidal meningitis in HIV-infected patients: analysis of 14 cases. *Clin. Infect. Dis.* **25,** 673–676 (1997).
6. Islam, Z., Harkema, J. R. & Pestka, J. J. Satratoxin G from the black mold *Stachybotrys chartarum* evokes olfactory sensory neurons loss and inflammation in the murine nose and brain. *Environ. Health Perspect.* **114,** 1099–1107 (2006).
7. Hancock, R. E. W. & Sahl, H. G. Antimicrobial and host-defence peptides as new anti-infective therapeutic strategies. *Nature Biotechnol.* **24,** 1551–1557 (2006).
8. Oren, Z. *et al.* Structures and mode of membrane interaction of a short α helical lytic peptide and its diastereomer determined by NMR, FTIR and fluorescence spectroscopy. *Eur. J. Biochem.* **269,** 3869–3880 (2002).
9. Oren, Z. & Shai, Y. Cyclization of a cytolytic amphipathic α-helical peptide and its diastereomer: effect on structure, interaction with model membranes and biological function. *Biochemistry* **39,** 6103–6114 (2000).
10. Shai, Y. Mode of action of membrane active antimicrobial peptides. *Biopolymers (Pept. Sci.)* **66,** 236–248 (2002).
11. Fernandez-Lopez, S. *et al.* Antibacterial agents based on the cyclic D,L-α-peptide architecture. *Nature* **412,** 452–455 (2001).
12. Avrahami, D. & Shai, Y. Conjugation of a magainin analogue with lipophilic acids controls hydrophobicity, solution assembly and cell selectivity. *Biochemistry* **41,** 2254–2263 (2002)
13. Vives, E., Brodin, P. & Lebleu, B. A truncated HIV-1 TAT protein basic domain rapidly translocates through the plasma membrane and accumulates in the cell nucleus. *J. Biol. Chem.* **272,** 16010–16017 (1997).
14. Ho, A., Schwarze, S. R., Mermelstein, S. J., Waksman, G. & Dowdy, S. F. Synthetic protein transduction domains: enhanced transduction potential *in vitro* and *in vivo*. *Cancer Res.* **61,** 474–477 (2001).
15. Fawell, S. *et al.* TAT-mediated delivery of heterologous proteins into cells. *Proc. Natl Acad. Sci. USA* **91,** 664–668 (1994).
16. Turner, J. J. *et al.* RNA targeting with peptide conjugates of oligonucleotides, siRNA and PNA. *Blood Cells Mol. Dis.* **38,** 1–7 (2007).
17. Pappalardo, J. S. *et al.* Improved transfection of spleen-derived antigen-presenting cells in culture using TATp-liposomes. *J. Control. Rel.* **134,** 41–46 (2009).
18. Schwarze, S. R., Ho, A., Vocero-Akbani, A. & Dowdy, S. F. *In vivo* protein transduction: delivery of a biologically active protein into the mouse. *Science* **285,** 1569–1572 (1999).
19. Santra, S. *et al.* Rapid and effective labeling of brain tissue using TAT-conjugated CdS: Mn/ZnS quantum dots. *Chem. Commun.* **25,** 3144–3146 (2005).
20. Liu, L. H. *et al.* Biologically active core/shell nanoparticles self-assembled from cholesterol-terminated PEG–TAT for drug delivery across the blood–brain barrier. *Biomaterials* **29,** 1509–1517 (2008).
21. Futaki, S. *et al.* Arginine rich peptides: an abundant source of membrane permeable peptides having potential as carriers for intracellular protein delivery. *J. Biol. Chem.* **276,** 5836–5840 (2001).
22. Wender, P. A. *et al.* The design, synthesis and evaluation of molecules that enable or enhance cellular uptake: peptoid molecular transporters. *Proc. Natl Acad. Sci. USA* **97,** 13003–13008 (2000).
23. Weiss, R. G. Thermotropic liquid crystals as reaction media for mechanistic investigations. *Tetrahedron* **44,** 3413–3475 (1988).
24. Lee, M., Rentz, J., Han, S.-O., Bull, D. A. & Kim, S. W. Water-soluble lipopolymer as an efficient carrier for gene delivery to myocardium. *Gene Therapy* **10,** 585–593 (2003).
25. Li, C., Peters, A. S., Meredith, E. L., Allman, G. W. & Savage, P. B. Design and synthesis of potent sensitizers of gram-negative bacteria based on a cholic acid scaffolding. *J. Am. Chem. Soc.* **120,** 2961–2962 (1998).
26. Dai, S., Ravi, P., Leong, C. Y., Tam, K. C. & Gan, L. H. Synthesis and aggregation behavior of amphiphilic block copolymers in aqueous solution: di- and tri-block copolymers of poly(ethylene oxide) and poly(ethyl acrylate). *Langmuir* **20,** 1597–1604 (2004).
27. Whittaker, M. R., Urbani, C. N. & Monteiro, M. J. Synthesis of linear and 4-arm star block copolymers of poly(methyl acrylate-b-solketal acrylate) by SET–LRP at 25 °C. *J. Polym. Sci. A* **46,** 6346–6357 (2008).
28. Jung, H. J., Park, Y., Hahm, K. S. & Lee, D. G. Biological activity of TAT (47–58) peptide on human pathogenic fungi. *Biochem. Biophys. Res. Commun.* **345,** 222–228 (2006).
29. Hyde, A. J., Parisot, J., McNichol, A. & Bonev, B. B. Nisin-induced changes in *Bacillus* morphology suggest a paradigm of antibiotic action. *Proc. Natl Acad. Sci. USA* **103,** 19896–19901 (2006).
30. Cho, S. *et al.* Structural insights into the bactericidal mechanism of human peptidoglycan recognition proteins. *Proc. Natl. Acad. Sci. USA* **104,** 8761–8766 (2007).
31. Chan, D. I., Prenner, E. J. & Vogel, H. J. Tryptophan- and arginine-rich antimicrobial peptides: Structures and mechanisms of action. *Biochim. Biophys. Acta* **1758,** 1184–1202 (2006).
32. Neuwelt, E. A. Mechanisms of disease: the blood–brain barrier. *Neurosurgery* **54,** 131–141 (2004).

Acknowledgements

The authors would like to thank J. Lu, K. Guo and S. Liu for helpful discussions. The authors are also grateful to the Clinical Testing Center, College of Medicine, Zhejiang University, P.R. China, for analysis of ALT, AST, total bilirubin, direct bilirubin, creatinine and urea nitrogen levels of the blood samples. This work was funded by the Institute of Bioengineering and Nanotechnology, Agency for Science, Technology and Research, the National Basic Research Program 973 of P.R. China (grant no. 2007cb513003) and the State Key Laboratory for Diagnosis and Treatment of Infectious Diseases, College of Medicine, Zhejiang University, P.R. China (grant no. 2008A05).

Author contributions

Y.Y.Y. oversaw the project. Y.Y.Y. and L. Liu designed the peptides and peptide nanoparticles. L. Liu and J.T.P.K. synthesized and characterized the peptide nanoparticles. L. Liu, K.X. and H.W. performed the *in vitro* experiments. L.L., K.X., H.W. and W.F. contributed to the *in vivo* experiments and data analysis. Y.Y.Y. wrote the paper with contributions from L. Liu. The other authors gave suggestions to improve the presentation of the paper and prepared the Methods section.

Additional information

Supplementary information accompanies this paper at www.nature.com/naturenanotechnology. Reprints and permission information is available online at http://npg.nature.com/reprintsandpermissions/. Correspondence and requests for materials should be addressed to Y.Y.Y. and L.L.